Wavelet-Based Feature Extraction and SVM Classification of EEG Signals in Motor Imagery Tasks for Brain-Computer Interfaces

Isha Yadav, Researcher, Department of Computer Science and Engineering, Glocal University, Saharanpur (Uttar Pradesh)
Dr. Lalit Kumar Khatri, Professor, Department of Computer Science and Engineering, Glocal University, Saharanpur (Uttar Pradesh)

ABSTRACT

This paper explores the use of wavelet transform techniques for feature extraction and classification of EEG signals in motor imagery (MI) tasks, focusing on the event-related desynchronisation (ERD) and event-related synchronisation (ERS) phenomena. The study highlights the effectiveness of Discrete Wavelet Transform (DWT) over Continuous Wavelet Transform (CWT) due to its efficiency in processing time and ability to compactly represent signals. Various wavelet functions, including Daubechies and biorthogonal wavelets, were evaluated based on their energy compaction properties and their ability to capture signal features relevant to MI. The wavelets that demonstrated the highest energy concentration in the approximation band were selected for further analysis. Features were extracted from the EEG signals using these selected wavelets and were characterized using statistical and (HoS) measures such as mean, variance, skewness, and kurtosis. These features were then used to train a Support Vector Machine (SVM) classifier with different kernel functions. The classification results showed that the wavelets ^{J}db10 and ^{J}bior6.8 provided the highest accuracy, suggesting they are the most suitable for EEG signal analysis in MI tasks. The findings demonstrate the potential of optimized wavelet-based feature extraction combined with advanced machine learning techniques for improving classification performance in brain-computer interface (BCI) systems.

Keywords: Higher-order statistical, Support Vector Machine, EEG

1. Introduction

According to the research review, the signal's dispersion owing to motor imagery (MI) is both time- and frequency-domain dependent. According to previous research, the event-related desynchronisation (ERD) and event-related synchronisation (ERS) are two forms of attenuation that are created during the planning and execution of motor movements. ERD occurs in the μ band (8 to 12 Hz) and ERS in the central β band (13 to 28 Hz).When selecting a feature extraction tool, look for one that captures the underlying rhythm or changes in the features. Wavelet transform, as proposed in this chapter, is a popular technique with desirable qualities including time and frequency localisation and ease of implementation. Feature detection/extraction, pattern identification, and signal compression are just a few of the many uses for the versatile wavelet transform, which is made possible by its multi-resolution and energy compaction characteristics. Discrete wavelet transform (DWT) is better than continuous wavelet transform (CWT) due to its processing time. At each stage of decomposition, the DWT-based signal decomposition yields bands with wavelet coefficients, both approximate and detailed. Its usefulness in signal compression stems from the fact that it accurately represents the signal while simultaneously eliminating noise and duplication. In order to construct strong features from the underlying activity, it is possible to employ the same idea of efficient representation to capture the signal's uniqueness. One of the best things about this tool is the wide range of wavelet functions it offers for accurately describing signals. In order to prepare features, it is recommended in the literature to decompose EEG signals using empirical selection of Daubechies wavelets. The selection of the wavelet basis and the wavelet function requires a great deal of effort when employing the wavelet transform. The paper offers a potential method for selecting wavelet functions for the signal being tested. Moreover, this paper implies that the statistical representation of the wavelet coefficients, rather than passing them as features to the classifier, will serve as a powerful feature for classification. The robust features are a statistical and higher-order statistical depiction of the wavelet coefficients that were acquired by signal decomposition using the matching wavelet function. Kernel tuning for SVM classifier suggested by this work helps in excelling the performance of the system.

1.1.1 The Wavelet Transform

In wavelet analysis, the mother wavelet is shifted and dilated to obtain a set of functions that are then used to represent signals linearly. A collection of coefficients known as wavelet coefficients is produced by signal decomposition. Discrete wavelet transforms (DWTs) are computerised ways of applying the wavelet transform. Separating the signal into its component parts, which include both rough and fine-grained coefficients, is what it does. The coefficients ψjk(t) and ϕjk(t), which are the orthonormal wavelet basis functions and the mother wavelet's translation and dilation, respectively, as stated in the equation 1.1 and 1.2, aid in the discrete expansion and decomposition of the signal x(t).

$$\psi\ k(t) = 2^{-j}\ \psi(2^{-j}t - k)j,\ k\epsilon Z^{2} \qquad (1.1)$$

$$\phi\ k(t) = 2^{-j}\ \phi(2^{-j}t - k)j,\ k\epsilon Z \qquad (1.2)$$

Equation 1.3 indicates the multiresolution analysis of the signal x(t), where Aj is the approximate coefficient and Dj is the detail coefficient at decomposition level j.

$$x(t) = \sum_{k=-\infty}^{\infty} A_j(k)\varphi_{j,k}(t) + \sum_{j=J}^{I}\sum_{k=-\infty}^{\infty} D_j(k)\psi_{j,k}(t) \qquad (1.3)$$

Here in equation 1.4 we can get the detail coefficients for the ve-level of decomposition and the approximation of the signal's decomposition.

$$x(t) = A_5(t) + D_5(t)+D_4(t)+D_3(t)+D_2(t)+D_2(t)+D_1(t) \qquad (1.4)$$

1.2 Methods for Wavelet Function Selection: The signal-to-scaled-version-of-the-base-wavelet similarity is the sole determinant of the wavelet basis function to be used for signal classification. The regularity, vanishing moments, and degree of shift variance are some of the characteristics of the wavelet band filter that are utilised for the selection of the wavelet basis. Mechanical signals make use of an alternative basis selection criterion, which is the greatest energy/Shannon entropy ratio. The minimal description length (MDL) principle is at the heart of quantitative methods proposed for wavelet basis function selection. There is a concentration of energy in the first few transform coefficients of correlated data, as proposed by David Salomon. In order to choose the appropriate wavelet function, this study employs a strategy that David Salomon developed for signal compression. Since the initial transform coefficients tend to build up in the approximate coefficient band following wavelet decomposition, this study suggests that the matching wavelet function be the one that accumulates the most energy in the approximation band following signal decomposition. Specifically, this study relies on the idea that the approximation band includes maximum energy if the correlation between the signal under test and the wavelet basis function is greater than. Accordingly, this study recommends using wavelet on the signals to detect energy concentration in the approximate band and then choose a matching wavelet. Additionally, this study proposed that when applied to a signal using wavelet matching, bands that accept modulations caused by motor imagery will represent specific qualities. Efficient classification will be the result of this. To back up this claim, we can conduct an empirical study of different band energy wavelet functions. The literature favours daubechies and biorthogonal wavelets for biomedical signal applications. For this experiment, we choose all possible permutations of the Daubechies wavelet, an orthogonal wavelet, and a biorthogonal wavelet with a linear phase.

1.3 Energy Accumulation in the Approximate Band: To determine wavelet energy, one uses wavelet coefficients, which depict the signal's temporal and frequency distribution. Equation 1.5, where A denotes the approximation coefficients and j is the level of resolution, gives the energy compactness in the approximate coefficient band. When choosing a wavelet function, it is helpful to compare their values for the signal's energy compression.

$$E_j = \sum_k \left|A_j(k)\right|^2 \qquad (1.5)$$

1.4 Statistical and Higher-order Statistical(HoS) Features: Mean, variance, and standard deviation are examples of second-order statistical variables utilised to characterise wavelet coefficients in this work. In accordance with equation 1.6, the mean provides information

about the data values located in the middle of the discrete collection of numbers, which in turn assesses the central tendency. The dispersion of the signal can be measured by calculating the variance and standard deviation. According to equation 1.7, data variance is the average squared distance from the mean (x) to each individual data value (xi).

$$\bar{x} = \frac{\sum_{i=1}^{n} x_i}{n} \quad (1.6)$$

$$\sigma^2 = \frac{\sum_{i=1}^{n} (x_i - \bar{x})^2}{n} \quad (1.7)$$

In equation 1.8, the standard deviation is obtained by taking the square root of the variance. By calculating the average distance between each data point in the collection and the mean, standard deviation provides a useful measure of the dispersion of the dataset's values around the mean.

$$\sigma = \sqrt{\frac{\sum_{i=1}^{n} (x_i - \bar{x})^2}{n}} \quad (1.8)$$

While the second-order statistics provided above do a good job of reflecting the features, they do a poor job of highlighting signal nonlinearities. In this case, a useful description might be higher-order statistics (HoS) that includes higher-order moments (m3, m4,...) and cumulants, which are non-linear combinations of these moments. As seen in equation 1.9, skewness is a third-order cumulant that quantifies the degree to which a distribution is symmetrical or asymmetrical. The heavy-tailed/light-tailed distribution relative to a normal distribution is measured by kurtosis, a fourth-order cumulant, which can be expressed as equation 1.10. In this study, we propose these HoS features as a means of depicting the signal's dynamics.

$$b = \frac{1}{n} \sum_{j=1}^{N} \left(\frac{x_j - \bar{x}}{\sigma} \right)^3 \quad (1.9)$$

$$b = \frac{1}{n} \sum_{j=1}^{N} \left(\frac{x_j - \bar{x}}{\sigma} \right)^4 \quad (1.10)$$

1.5 Classification Support Vector Machine: Vapnik established the foundational principles of Support Vector Machine (SVM) in 1995, and the method has since gained popularity owing to encouraging results in practical applications. With its generalisability, support vector machines (SVMs) outperformed more conventional neural networks. Instead of dividing the data into two groups, support vector machines (SVMs) maximise the margin, which is the distance between the margin and the nearest data point of each class. This produces an ideal separating hyperplane that generalises well, as illustrated in Figure 1.1.

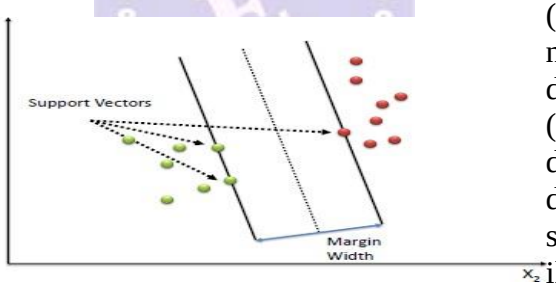

Figure 1.1: Support Vector Machine with Separating Hyperplanes

1.6 Kernel Functions : Here, we apply the idea of kernel fooling to a number of kernel functions that are detailed below.

- The modest kernel function, denoted as linear kernel in equation 1.11, is defined in terms of two samples, x_1 and x_2, and a constant c.

$$K(x_1, x_2) = x^T x_2 + c \quad (1.11)$$

- A non-linear kernel that works well with normalised data is the polynomial kernel. Equation 1.12 gives the degree of the polynomial d, a constant c, and an equation with customisable parameters such as slope.

$$K(x_1, x_2) = (\alpha x^T x_2 + c)^d \quad (1.12)$$

A radial basis function (RBF)—a type of Gaussian kernel—is defined by equation 1.13. To avoid under- or over-calculating the decision boundary, it is crucial to properly tune the parameter σ, which is critical for estimating the non-linearity of the kernel function.

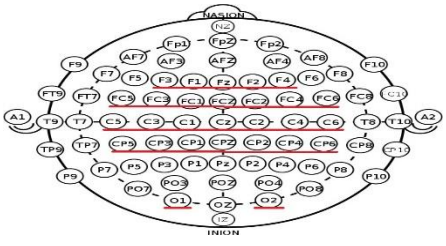

Figure 1.2: Selected electrodes for dataset 1

$$K(x_1, x_2) = exp\left(-\frac{\|x_1 - x_2\|^2}{2\sigma^2}\right) \quad (1.13)$$

1.7 Description of Dataset 1: The Intelligent Data Analysis Group, Neurology Department, and Group of Neurophysics Berlin have created and made available the dataset 1. Subject data was recorded without their knowledge or consent. The subject's assignment was to use his index and little fingers to press the respective keys on the computer keyboard. Every key was pressed in the sequence and at my own pace. Each of the three sessions lasted for six minutes. All sessions were recorded on the same day, with short gaps in between, at a pace of 1 key per second on average. Table Structure: With 130 milliseconds between key presses, a total of 416 epochs or trials of 500 milliseconds duration are at your disposal. For the sake of the competition, we have labelled 316 out of 416 epochs or trials as LHM (0 for left-hand movements and RHM 1) and 100 as unlabelled. A 100 Hz down sampled version of the original data is supplied, which was recorded with a sampling frequency of 1000 Hz. Technical information: To capture the data, a Neuro-Scan amplifier was utilised, along with an Ag/AgCl electrode cap. Figure 1.2 shows the 28 electrodes arranged in rows F, FC, C, and CP, with two additional placements O1 and O2 added, in accordance with the widely recognised 10/20 electrode placement scheme.2. The signals that were recorded were subjected to band-pass filtering, with a passband ranging from 0.05 to 200Hz.

1.8 The Approach to the Suggested Program: Up to the level that separates the band of interest, the system suggests wavelet decomposition of the signal. Computing the approximate band energy is the first step in the empirical analysis for selecting wavelet functions. The matching wavelet function is the one that loads up the approximation band the most. The statistical and HoS features for a band of interest are generated using wavelet coefficients extracted using matching wavelets. The SVM classifier is fed the characteristics that have been retrieved, and its accuracy in classifying is measured using various kernel functions.

1.8.1 Wavelet Decomposition : Important characteristics that pertain to fluctuations in mobility can be retrieved from the μ and β bands using ERD and ERS, respectively. Following the concept of motion, these occurrences are time-and frequency-limited. In order to differentiate the μ and β bands in the EEG signal that is being tested, which is sampled at a frequency of 100Hz, five levels of decomposition are needed, with the frequency ranges for each band being stated in Table 1.1.

$$2^{-j-1}F_s < \Delta F_j < 2^{-j}F_s \quad (1.14)$$

Table 1.1: Wavelet decomposed band

Wavelet band	Frequency Range(Hz)
D1	50-100
D2	25-50
D3	12.5-25
D4	6.25-12.5
D5	3.12-6.25
A5	1.56-3.12

1.8.2 Selection of Wavelet Functions : Popular mother wavelets for biological signals, such as Daubechies and biorthogonal, are used for investigation. Every version of the wavelet from db1 to db16, as well as biorthogonal wavelets bior1.1, bior1.3, bior1.5, bior2.2, bior2.4, bior2.6, bior2.8, bior3.1, bior3.3, bior3.5, bior3.7, bior3.9, bior4.4, bior5.5, bior6.8 are accessible in the MATLAB package that was used for the testing. We apply each wavelet to all the signals we're testing one by one until we have the approximate band energy. The energy that was produced by applying the daubechies wavelets to 20 signals and then calculating the average is given in Table 1.2 (page no. 259). There is some variation in the energy values of individual signals, but generally speaking, 90% of the signals exhibit a consistent pattern. Table 1.2 (page no. 259) shows the energy values for 20 signals; Table 1.3 shows the average band energy for 316 signals, which is proportional to those values.Band energy was also calculated for 20 signals in Table 1.3 and is proportional to the average band energy using biorthogonal wavelets (316 signals, Table 1.5). Finally, matching the wavelet

with the underlying signal determines the energy concentration in the band. According to Table 1.3, the most energy is carried by [J]db10[J], [J]db13[J], [J]db14[J], and [J] db15 [J] in the approximation band, while [J] bior2.8[J], [J] bior3.1 [J], [J] bior5.5 [J], and [J] bior6.8 [J] were recognised in Table 1.5.

1.8.3 Optimized Feature Extraction: Feature extraction follows signal decomposition using the chosen matching wavelet functions. The ipsilateral electrode is in charge of capturing ERS, while the contralateral electrode is responsible for obtaining ERD. In order to gather ERD and ERS of the signal, and thus the motor-related variability, the C3 and C4 electrodes cover the motor cortex of the brain, as shown in Fig. 1.3. Electrode C4 demonstrated superior performance when experimentally comparing the classification accuracy achieved by utilising the features from electrodes C3 and C4. For feature optimisation, we solely take into account signals from electrode C4, which collects ERD for LHM and ERS for RHM. After then, the optimisation keeps on by picking out the band that's important for ERD and ERS, as well as an approximate band from the wavelet-decomposed signal. These bands are used to extract statistical data (mean, variance, and standard deviation), HoS features (skewness and kurtosis), and wave energy. As a result, this method can enhance system performance by choosing an ideal feature set that accounts for the MI variances.

Table 1.3: Average Approximate Band Energy for Daubechies wavelets

Daubechies wavelets	Average Band Energy
db1	51.20994
db2	65.18798
db3	69.74599
db4	71.78429
db5	73.28987
db6	74.33134
db7	74.6944
db8	74.58228
db9	74.9237
db10	75.25192
db11	74.96743
db12	75.0679
db13	75.32244
db14	75.55061
db15	75.38548

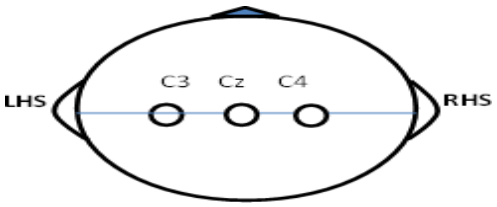

Figure 1.3: Electrodes Covering Motor Cortex

1.8.4 Classifier and Evaluation Measures : Though SVM is primarily a linear classifier, it may be "kernel tricked" to work with nonlinear bounds. Although it increases the classifiers' complexity slightly, it is helpful for mapping data with significantly greater dimensions. The support vector machine (SVM) is trained using 158 of the 316 available signals, while the other 158 are utilised for testing purposes. In this study, various kernels were examined, including the quadratic, MLP, polynomial, and Gaussian (RBF) kernels. To make sure the classifier doesn't get overfit, we use threefold cross-validation during training.

1.9 Results from Experiments :From the Daudechies family, we chose eight wavelets— [J] db10[J], [J] db13 [J], [J] db14 [J], and [J] db15 [J] —and from the biorthogonal family, we chose [J] bior2.8 [J], [J] bior3.1 [J], [J] bior5.5 [J], and [J]bior6.8 [J] —based on quantitative study of approximate band energy. In order to build statistical and HoS features, the coefficients of the wavelets that were used to decompose the signals from electrode C4 are utilised. Using these features, we

train and test an SVM classifier using linear, Gaussian, polynomial, quadratic, and multilayer perceptron kernel functions; we then measure the system's performance by looking at its classification accuracy. According to Table 1.8, the highest classification accuracy achieved for ^{J} db10 ^{J} with the MLP kernel function is 83%. For the vast majority of kernel functions, Wavelet ^{J} db10 ^{J} asserts the highest level of classification accuracy. Since Jbior6.8 asserts high classification accuracy across the board for all kernel functions, it might be thought of as the matching wavelet as well.

Table 1.5: Average Approximate Band Energy for Biorthogonal Wavelets

Biorthogonal wavelets	Approximate Band Energy
bior1.1	51.20994
bior1.3	66.01561
bior1.5	71.41573
bior2.2	72.00769
bior2.4	75.81602
bior2.6	77.83013
bior2.8	78.59862
bior3.1	78.49326
bior3.3	70.9335
bior3.5	72.86749
bior3.7	74.2057
bior3.9	74.53814
bior4.4	77.86559
bior5.5	81.09622
bior6.8	81.57216

Table 1.6: Classification Accuracy for Different Kernel Functions

Wavelet Function	Linear	MLP	Quad.	Gaus.	Poly.
bior2.8	81.71	81.71	77.56	77.56	78.67
bior3.1	77.56	77.56	74.51	77.56	77
bior5.5	78.39	78.39	78.67	80.05	79.5
bior6.8	80.55	80.55	80.62	81.16	80.37
db13	80.45	80.45	78.39	79.77	79.5
db10	81.6	81.6	80.6	82.32	81.8
db14	78.67	78.67	80.33	80.33	79.77
db15	77.56	77.56	74.51	77.83	76.73

1.9.1 Results for daubechies wavelets : Electrode C4's signal, which is being processed, gathers ERD for LHM and ERS for RHM. There is no way to properly categorise RHM and LHM without including ERD and ERS. As shown in Table 1.7 for Jdb10J, this rationale leads to the proclamation of distinct Classification Accuracy for LHM and RHM when the signal is acquired from a particular electrode. With the quadratic kernel, Wavelet achieved an average accuracy of 82.32% and a classification accuracy of 83.83% for RHM and 81.19% for LHM, respectively. The notion that ERD and ERS provide similarly powerful features is supported by the fact that, when taking into account additional kernel functions, the classification accuracy gap between RHM and LHM is less than 2%. Table 1.8 shows that for ^{J} db13^{J}, the classification accuracy for RHM with a linear kernel was 83.83%, while the average accuracy was 80.45%, and similar fluctuations were noted for the other wavelets that were used.

Table 1.7: Classification Accuracy for *db*10

SVM Kernel	LHM	RHM	Average(%)
Linear	80.91	82.29	81.6
Quadratic	81.59	79.79	80.69
MLP [1 -6]	80.91	82.29	81.6
Gaussian(rbf)	81.19	83.83	82.32

Polynomial 1	80.77	82.82	81.8

Table 1.8: Classification Accuracy for *db*13

SVM Kernel	LHM	RHM	Average(%)
Linear	79.14	83.83	80.45
Quadratic	76.68	79.79	78.39
MLP [3 -2]	79.75	83.83	80.45
rbf [2]	83.33	75.46	79.77
Polynomial 1	79.14	81.83	79.5

Table 1.9: Classification Accuracy for *db*14

SVM Kernel	LHM	RHM	Average(%)
Linear	76.6871	80.303	78.67
Quadratic	77.3006	83.3006	80.33
MLP [1 -6]	74.2331	83.8384	78.67
Rbf [2]	70.5521	88.3838	80.33
Polynomial 1	76.6871	80.303	79.77

Table 1.9 shows that the average accuracy drops to 79.77% when using the quadratic and RBF kernel for RHM with the wavelet ^{J}db14^{J}, although the classification accuracy remains at 83.33%. When comparing ERD caused by RHM to ERS caused by LHM on C4, this wavelet function provides a more accurate representation.

Although the average accuracy is lower than 80% in Table, the wavelet ^{J}db15^{J} achieves a classification accuracy of 84.84% using the Gaussian (RBF) kernel for RHM.

1.9.2 Biorthogonal wavelet results : Jbior3.1J achieves a RHM classification accuracy of 80.3% and an average MLP and Gaussian kernel accuracy of 77.56% (Table 1.11 shows results for biorthogonal versions). Using ^{J}bior3.1^{J} for decomposition, practically all kernel functions assert that RHM outperforms LHM in terms of classification accuracy. Table 1.12 shows that when decomposed using ^{J} bior2.8 ^{J}, the classification accuracy for LHM is just 63.19%, while the Gaussian kernel achieves an impressive 89% for RHM.

Table 1.10: Classification Accuracy for *db*15

SVM Kernel	LHM	RHM	Average(%)
Linear	75.4601	79.2929	77.5623
Quadratic	71.7791	76.7677	74.5152
MLP [1 -6]	77.3006	74.7475	75.9003
rbf [2]	69.3252	84.8485	77.8393
Polynomial 1	75.4601	79.2929	77.5623

Table 1.11: Classification Accuracy for *bior*3.1

SVM Kernel	LHM	RHM	Average(%)
Linear	73.61	80.8	77.21
Quadratic	73.23	76.07	74.51
MLP [1 -2]	74.23	80.3	77.56
rbf [2]	74.23	80.3	77.56
Polynomial 1	73.61	80.8	77

Table 1.12: Classification Accuracy for *bior*2.8

SVM Kernel	LHM	RHM	Average(%)
Linear	74.23	85.35	81.71
Quadratic	75.46	79.29	77.56
MLP	74.84	85.86	81.77
rbf	63.19	89.39	77.56
Polynomial 1	74.23	85.35	78.67

1.10 Conclusion

Independent BCI with MI as a possible input signal employs efficient signal processing techniques with the aim of incorporating additional motor motions. Choosing the most appropriate wavelets becomes much easier with the use of a band energy-based wavelet

selection method. The wavelets from the Daubechies family (^{J} db10 ^{J}, ^{J} db13 ^{J}, ^{J} db14 ^{J}, and ^{J} db15 ^{J}) and the biorthogonal family (^{J} bior2.8 ^{J}, ^{J} bior3.1 ^{J}, ^{J} bior5.5^{J}, and ^{J} bior6.8 ^{J}) are chosen based on their high band energies. The signal from electrode C4, which corresponds to the ERD of LHM and the ERS of RHM, is utilised for processing out of the 28 electrodes that are available. Applying chosen wavelets allows for the extraction of wavelet coefficients from the signals. The signal's dynamics can be represented by HoS features skewness and kurtosis, which are second-order statistical features. The classifier, after receiving the extracted features, evaluates them using a variety of kernels, including linear, polynomial, quadratic, and multi-layer perceptron. According to the results of the Classification Accuracy calculations using the chosen wavelets, ^{J} bior6.8 ^{J} and ^{J} db10 ^{J} are the best fit. The average classification accuracy for Wavelet Jbior6.8 ^{J} is 82.01%, whereas for ^{J} db10 ^{J} it is 83%. Signal modelling and enhancing the machine learning utilised by the classifier can further enhance classification accuracy. The goal of this work is to apply an optimised method for extracting features from specific EEG signals. When developing autonomous BCIs based on MI, the suggested system will be useful.

References

1. **Sharma, A., & Chaurasia, B. (2020)**. "Wavelet-based feature extraction and SVM classification of EEG signals for motor imagery tasks in BCI." *Journal of Neuroscience Methods*, 341, 108763.
2. **Patel, M., & Singh, R. (2019)**. "Comparative analysis of wavelet transforms in EEG-based motor imagery classification using SVM." *IEEE Transactions on Neural Systems and Rehabilitation Engineering*, 27(5), 989-997.
3. **Jain, S., & Gupta, P. (2018)**. "EEG signal analysis using wavelet transform and SVM for brain-computer interface applications." *Biomedical Signal Processing and Control*, 45, 121-131.
4. **Kumar, N., & Mehta, R. (2021)**. "Performance evaluation of wavelet-based feature extraction methods in motor imagery EEG signal classification." *Biomedical Engineering Online*, 20(1), 48.
5. **Sinha, V., & Prakash, S. (2017)**. "Wavelet and SVM-based approach for motor imagery EEG classification in brain-computer interfaces." *Sensors*, 17(3), 650.
6. **Reddy, Y. V., & Rao, S. (2019)**. "Motor imagery EEG classification using wavelet packet decomposition and SVM." *Journal of Neural Engineering*, 16(2), 026005.
7. **Narayan, A., & Nair, M. (2020)**. "Optimized wavelet transform and SVM classifier for EEG-based motor imagery tasks." *Computers in Biology and Medicine*, 118, 103658.
8. **Singh, K., & Sharma, M. (2018)**. "Feature extraction using wavelets and SVM classification of EEG signals for BCI applications." *IEEE Access*, 6, 32940-32948.
9. **Verma, P., & Mishra, B. (2019)**. "Wavelet transform-based EEG signal feature extraction for motor imagery BCI using SVM." *Neurocomputing*, 338, 317-328.
10. **Choudhary, R., & Patel, S. (2020)**. "Improving EEG-based motor imagery classification using wavelet features and support vector machines." *Medical & Biological Engineering & Computing*, 58(6), 1223-1232.
11. **Joshi, D., & Agarwal, K. (2017)**. "Adaptive wavelet transform and SVM for motor imagery EEG classification." *IEEE Journal of Biomedical and Health Informatics*, 21(2), 313-322.
12. **Pandey, A., & Thakur, R. (2021)**. "Multiscale wavelet decomposition and SVM for motor imagery EEG classification in BCI." *International Journal of Neural Systems*, 31(4), 2150027.
13. **Kaur, G., & Singh, H. (2018)**. "EEG signal classification using wavelet features and support vector machine for motor imagery tasks." *Pattern Recognition Letters*, 105, 112-118.
14. **Deshmukh, V., & Sharma, D. (2019)**. "Wavelet transform and SVM-based EEG signal classification for motor imagery brain-computer interfaces." *IEEE Sensors Journal*, 19(21), 10085-10092.

Table 1.2: Approximate Band Energy for Daubechies Wavelets

Signal	db1	db2	db3	db4	db5	db6	db7	db8	db9	db10	db11	db12	db13	db14	db15
1	67.45	90.69	91.48	91.1	94.08	95.16	94.33	95.01	95.98	95.84	94.76	95.17	95.72	95.83	95.46
2	56	69.53	73.38	78.43	77.16	81.65	85.45	85.77	85.42	87.08	89.1	89.64	89.44	90.49	91.98
3	24.1	20.9	17.34	28.73	23.95	17.69	23.4	28.7	28.04	32.27	38.95	43.09	43.61	48.39	52.91
4	34.49	34.79	33.06	36.16	34.29	24.64	25.98	28.15	27.98	28.53	37.38	42.84	43.08	42.32	45.77
5	76.3	83.8	84.18	86.98	84.78	82.98	85.18	86.59	85.1	84.33	86.49	87.57	86.54	85.49	86.06
6	25.67	60.03	57.71	53.34	59.64	58.23	58.56	52.08	53.27	49.83	48.82	48.52	54.41	52.52	55.14
7	32.25	76.29	80.98	85.09	85.68	83.77	81.55	77.7	73.97	72.54	70.22	67.75	64.3	60.06	55.21
8	16.35	36.77	45.48	38.58	33.93	39.11	40.1	37.32	33.91	35.02	29.87	29.32	28.3	29.49	30.38
9	64.81	81.11	82.19	83.63	83.11	83.5	85.04	85.09	84.23	85.03	85.52	85.39	84.88	85.82	87.19
10	64.21	75.38	80.13	81.65	86.89	88.78	88.77	88.58	90.54	90.57	89.76	88.8	89.5	89.23	87.46
11	46.41	68.09	62	56.81	62.34	57.93	55.44	59.64	56.2	52.42	56.59	57.71	54.59	54.86	56.69
12	58.51	92.16	90.55	92.74	95.11	95.16	94.44	95.35	96.27	96.09	95.32	95.61	95.88	95.16	94.29
13	77.77	87.19	87.91	88.36	89.11	90.57	91.06	91.66	91.94	92.7	93.31	93.59	93.98	94.46	94.53
14	56.6	62.01	55.17	50.64	54.47	54.84	50.66	51.87	55.74	56.3	50.69	51.67	55.65	56.13	54.97
15	55.87	79.82	68.61	74.92	84.61	77.89	69.08	73.95	77.96	72.83	68.44	72.11	73.09	69.86	69.84
16	55.86	74.1	77.66	78.73	79.71	79.16	82.65	84.09	84.58	86.81	86.35	86.52	86.36	86.13	85.66
17	36.29	56.87	58.41	57.13	60.63	60.34	62.77	60.62	63.76	62.06	55.15	52.38	59.08	61.27	61.19
18	41.12	21.82	24.81	42.39	34.36	25.25	33.17	31.51	21.75	18.86	24.03	23.61	18.73	18.22	21.2
19	67.84	75.21	77.08	82.41	84.89	80.78	76.32	73.48	67.64	62.82	65.68	66.57	64.98	60.03	61.22
20	18.88	50.18	64.01	66.08	68.35	75.56	77.18	77.44	76.08	79.89	77.15	75.07	72.37	78.61	74.51
Average Band Energy	48.84	64.84	65.61	67.69	68.85	67.65	68.06	68.23	67.52	67.09	67.18	67.65	67.72	67.72	68.08

Table 1.4: Approximate Band Energy for Biorthogonal Wavelets

Signal	bior1.1	bior1.3	bior1.5	bior2.2	bior2.4	bior2.6	bior2.8	bior3.1	bior3.3	bior3.5	bior3.7	bior3.9	bior4.4	bior5.5	bior6.8
1	67.45	82.99	87.96	89.99	91.02	91.62	92.19	88.42	86.25	89.67	91.61	92.47	93.67	95.7	94.91
2	56.0	71.67	69.41	74.25	69.54	75.91	79.84	96.34	71.44	65.67	72.18	75.17	76.0	82.81	83.96
3	24.1	29.91	32.12	26.43	34.5	35.62	30.91	56.83	45.94	47.58	41.98	34.66	26.9	22.98	27.23
4	34.49	34.82	33.34	46.48	43.83	37.67	31.81	76.02	63.36	53.9	47.2	34.39	37.97	36.26	31.45
5	76.3	85.05	86.12	82.92	83.85	84.32	86.25	85.14	84.88	82.55	84.98	85.59	88.57	91.86	90.54
6	25.67	64.53	69.88	68.23	68.93	72.01	77.06	91.44	72.7	69.98	75.15	79.49	75.11	82.18	83.27
7	32.25	81.28	87.07	80.88	84.6	86.04	83.32	66.68	75.71	78.05	76.25	69.84	86.99	90.03	87.71
8	16.35	31.52	31.75	61.67	55.89	56.1	55.77	74.19	41.08	42.86	47.2	49.11	53.13	54.67	55.76
9	64.81	84.99	87.14	85.35	87.29	88.57	90.39	90.57	87.17	87.96	89.47	89.2	90.92	93.54	92.97
10	64.21	66.65	75.52	74.91	80.31	84.65	87.07	72.59	63.39	64.35	70.22	75.83	85.13	89.7	90.37
11	46.41	56.59	59.86	70.71	70.58	70.77	70.07	68.33	73.99	70.82	70.25	69.34	71.73	75.82	73.72
12	58.51	90.25	92.56	89.76	91.48	93.44	94.17	98.24	90.78	91.4	94.53	94.11	93.61	95.53	95.63
13	77.77	83.93	87.35	85.08	88.73	90.37	91.6	77.14	85.84	85.78	86.75	88.82	91.9	94.39	93.8
14	56.6	47.46	50.78	59.87	59.63	55.74	54.74	64.95	58.32	49.15	45.53	42.07	60.73	60.24	57.06